

Basement topography and sediment thickness beneath Antarctica's Ross Ice Shelf

M.D. Tankersley^{1,2}, H.J. Horgan¹, C.S. Siddoway³, F. Caratori Tontini^{2,4}, K.J. Tinto⁵

¹Antarctic Research Centre, Victoria University of Wellington, Wellington, New Zealand

²GNS Science, Lower Hutt, New Zealand

³Colorado College, Colorado Springs, CO, USA

⁴University of Genova, Genova, Italy

⁵Lamont-Doherty Earth Observatory, Columbia University, Palisades, NY, USA

Key Points:

- Aeromagnetic analysis reveals basement surface and evidence of fault-controlled extensional basins beneath Antarctica's Ross Ice Shelf
- Active faults at Siple Coast likely influence ice streams through control of geothermal heat, groundwater, and glacioisostatic adjustments
- A basement high beneath Ross Ice Shelf spatially coincides with a lithospheric boundary, with contrasting sedimentary basins on either side

Corresponding author: Matthew Tankersley, matthew.tankersley@vuw.ac.nz

17 **Abstract**

18 New geophysical data from Antarctica’s Ross Embayment reveal the structure and
 19 subglacial geology of extended continental crust beneath the Ross Ice Shelf. We use air-
 20 borne magnetic data from the ROSETTA-Ice Project to locate the contact between mag-
 21 netic basement and overlying sediments. We delineate a broad, segmented basement high
 22 with thin (0-500m) non-magnetic sedimentary cover which trends northward into the Ross
 23 Sea’s Central High. Before subsiding in the Oligocene, this feature likely facilitated early
 24 glaciation in the region and subsequently acted as a pinning point and ice flow divide.
 25 Flanking the high are wide sedimentary basins, up to 3700m deep, which parallel the Ross
 26 Sea basins and likely formed during Cretaceous-Neogene intracontinental extension. NW-
 27 SE basins beneath the Siple Coast grounding zone, by contrast, are narrow, deep, and
 28 elongate. They suggest tectonic divergence upon active faults that may localize geother-
 29 mal heat and/or groundwater flow, both important components of the subglacial sys-
 30 tem.

31 **Plain Language Summary**

32 The bedrock geology of Antarctica’s southern Ross Embayment is concealed by 100s
 33 to 1000s of meters of sedimentary deposits, seawater, and the floating Ross Ice Shelf. Our
 34 research strips away those layers to discover the shape of the consolidated bedrock be-
 35 low, which we refer to as the basement. To do this, we use the contrast between non-
 36 magnetic sediments and magnetic basement rocks to map out the depth of the basement
 37 surface under the Ross Ice Shelf. Our primary data source is airborne measurements of
 38 the variation in Earth’s magnetic field across the ice shelf, from flight lines spaced 10-
 39 km apart. We use the resulting basement topography to highlight sites of possible in-
 40 fluence upon the Antarctic Ice Sheet and to further understand the tectonic history of
 41 the region. We discover contrasting basement characteristics on either side of the ice shelf,
 42 separated by a N-S trending basement high. The West Antarctic side displays evidence
 43 of active faults, which may localize geothermal heat, accommodate movements of the solid
 44 earth caused by changes in the size of the Antarctic Ice Sheet, and control the flow of
 45 groundwater between the ice base and aquifers. This work addresses critical interactions
 46 between ice and the solid earth.

47 **1 Introduction**

48 The southern sector of Ross Embayment beneath the Ross Ice Shelf (RIS; area $\sim 480,000\text{km}^2$)
 49 is poorly resolved because the region is not accessible to conventional seismic or geophys-
 50 ical surveying. Rock exposures on land suggest that RIS crust consists of early Paleo-
 51 zoic post-orogenic sediments, intruded in places by mid-Paleozoic and Cretaceous gran-
 52 itoids (Luyendyk et al., 2003; Goodge, 2020). Since the mid-Cretaceous onset of exten-
 53 sion, grabens formed and filled with terrestrial and marine deposits, continuing into the
 54 Cenozoic (e.g. Sorlien et al., 2007; Coenen et al., 2019), as the Ross Embayment under-
 55 went thermal subsidence (Karner et al., 2005; Wilson & Luyendyk, 2009). The physiog-
 56 raphy of this region then responded to the onset of glaciation in the Oligocene (Paxman
 57 et al., 2019), coinciding with localized extension in the western Ross Sea until 11 Ma (Granot
 58 & Dymant, 2018). The Oligocene-early-Miocene paleo-landscape of the Ross Sea sector
 59 was revealed by marine seismic data (e.g. Brancolini et al., 1995; Pérez et al., 2021) and
 60 drilling that penetrated crystalline basement (DSDP Site 270; Ford & Barrett, 1975) (Fig-
 61 ure 3). Recognition of the role of elevated topography in Oligocene formation of the Antarc-
 62 tic Ice Sheet (DeConto & Pollard, 2003; Wilson et al., 2013) and the likely influence of
 63 subglacial topography upon ice sheet processes during some climate states (Austermann
 64 et al., 2015; Colleoni et al., 2018) motivated our effort to determine basement topogra-
 65 phy beneath the Ross Ice Shelf.

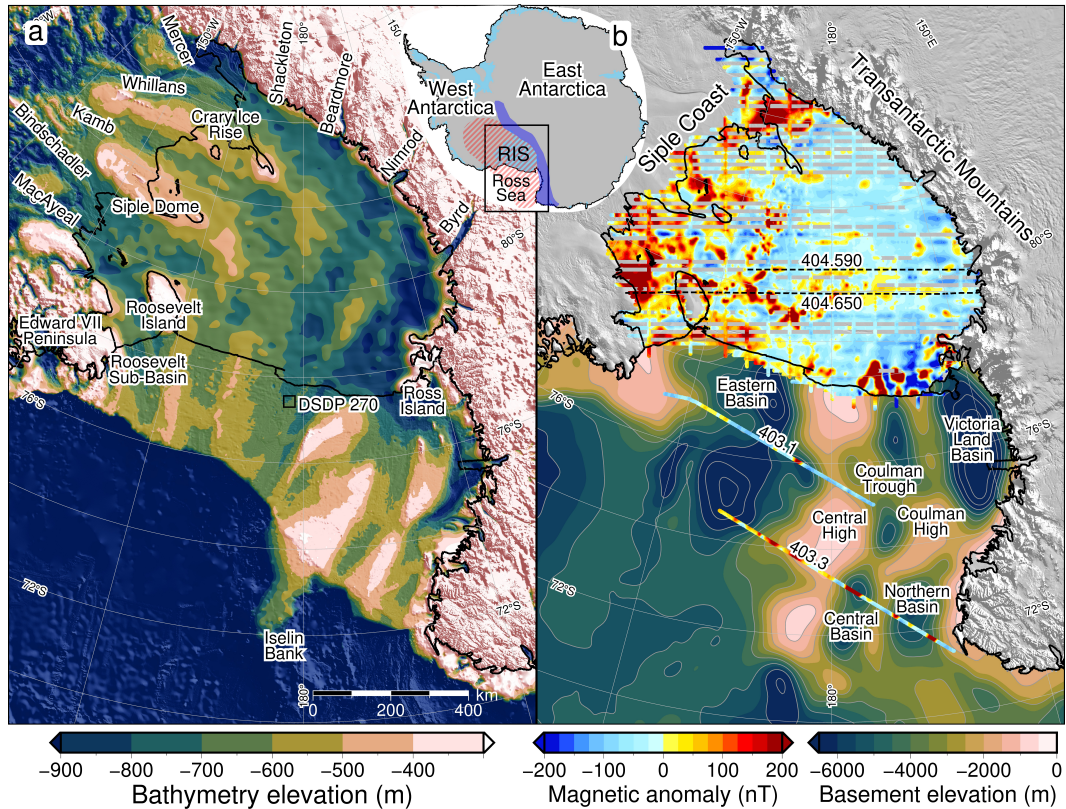


Figure 1. (a) Bathymetry and sub-ice bed elevations (Morlighem et al., 2020) including ROSETTA-Ice gravity-derived bathymetry (Tinto et al., 2019) beneath the Ross Ice Shelf (RIS). Labels include ice streams and outlet glaciers. (b) Basement depths from ANTOSTRAT marine seismic compilation in the Ross Sea (Brancolini et al., 1995) and airborne magnetic data from ROSETTA-Ice (over RIS) and Operation IceBridge (over Ross Sea). Inset map shows figure location, West Antarctic Rift System (hatched red), and Transantarctic Mountains (dark blue), and ice shelves (light blue). Shelf edge, grounding line, and coastlines in black (Rignot et al., 2013). MODIS imagery from Scambos et al. (2007).

Ice sheet dynamics are of high interest in the RIS region because its grounding zone (GZ) and pinning points (Still et al., 2019) buttress Antarctica’s second-largest drainage basin (Tinto et al., 2019). Our work in this sensitive region seeks to delimit the extent and geometry of competent basement because the margins of basement highs are sites of strong contrasts in permeability that influence the circulation of subglacial waters. A spectacular example of the confinement of subglacial water between the ice sheet and basement exists in ice radar profiles for the continental interior (Bell et al., 2011), but the hydrologic system is poorly known for subglacial sediment-filled marine basins that receive terrestrial freshwater influx (Siegert et al., 2018; Gustafson et al., 2021). Possible evidence that basement margins localize geothermal fluids or basinal waters, causing the advection of geothermal heat, comes from elevated values and significant spatial variability of measured geothermal heat flux (GHF) at points around the Ross Embayment (Begeman et al., 2017). Here we present the first map of magnetic basement topography and thickness of overlying non-magnetic sediments for the southern Ross Embayment, developed using ROSETTA-Ice (2015-2019) airborne magnetic data (Figure 1b, Tinto et al., 2019). Our work reveals three major sedimentary basins and a broad basement ridge that separates crust of contrasting basement characteristics.

2 Data and Methods

We applied Werner deconvolution (Werner, 1953) to estimate the depth to the top of the magnetic crust along ROSETTA-Ice flight lines at 10-km spacing (Figures 1b&S4). The approach assumes that sediments and sedimentary rocks produce significantly lower amplitude magnetic anomalies than underlying crystalline basement (Text S6). Here, Werner deconvolution is performed on 2D moving and expanding windows of aeromagnetic line data by isolating anomalies and solving for their source parameters (Birch, 1984). The resulting solutions are non-unique; each observed magnetic anomaly can be solved by bodies at multiple locations and depths by varying the source’s magnetic susceptibility and width. The result is a depth scatter of solutions (black dots in Figure 2), which we filtered based on magnetic susceptibility and binned to produce a basement surface (Text S1).

We implemented a 2-step tuning process that ties our RIS magnetic basement to well-constrained seismic basement in the Ross Sea, from the Antarctic Offshore Stratigraphy project (ANTOSTRAT) (Figure 1b, Brancolini et al., 1995). This involved using Operation IceBridge (OIB) airborne magnetic data (Cochran et al., 2014) collected over the RIS and Ross Sea. Minimizing misfits between OIB magnetic basement and ANTOSTRAT basement, as well as between OIB and ROSETTA-Ice magnetic basements, enabled tuning of our method to optimal basement depths (Figures 2, S2, S3e&f, Text S2-3).

Our RIS results (Figure S4) were merged with offshore ANTOSTRAT data (Brancolini et al., 1995) and smoothed with an 80km Gaussian filter to match the characteristic wavelengths of the Ross Sea basement (Text S4). The combined grid (Figure 3a) was then subtracted from bathymetry (Figure 1a, Text S5, Morlighem et al., 2020), to map basins and obtain the sediment thickness distribution for the Ross Embayment (Figure 3b).

We used basement features and geophysical anomaly patterns to infer regional scale faults beneath the RIS. Criteria used to locate faults include 1) high relief on the magnetic basement surface, 2) linear trends that cross zones of shallow basement, 3) high gradient gravity anomalies (Figure S1a) and 4) large contrasts in sediment thickness. Narrow, deep, linear basins are likely to be controlled by active faults (e.g. Finn, 2002; Drenth et al., 2019). We display the inferred faults upon a base map of crustal stretching factors (β -factor; the ratio of crustal thickness before and after extension, Figure 4a), using an initial crustal thickness of 38km (Müller et al., 2007), a continent-wide Moho model (An et al., 2015), and our basement surface as the top of the crust (Text S5).

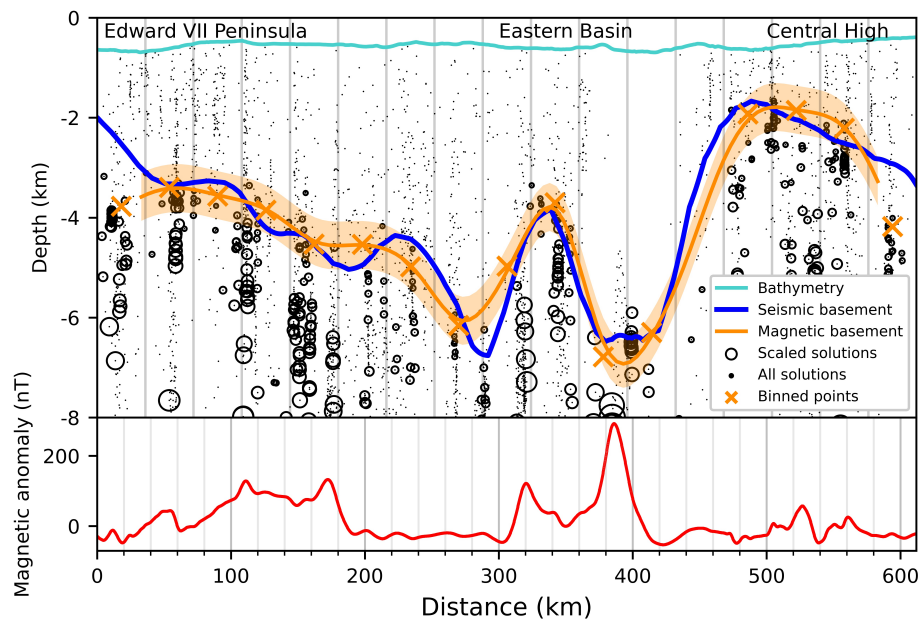


Figure 2. Ross Sea magnetic and seismic basement comparison. Operation IceBridge airborne magnetic data (lower panel) from segment 403-1 (Figure 1b) used in Werner deconvolution to produce magnetic basement (orange line with uncertainty band). Bathymetry from Fretwell et al. (2013). Seismic basement from ANTOSTRAT (Brancolini et al., 1995). See Text S2-S3 for a description of symbols.

3 Results

An almost continuous drape of sediment covers the RIS region (Figure 3b), with only $\sim 1\%$ of the area having $< 100\text{m}$ of sedimentary cover. Prominent beneath the midline of the RIS is a broad NNW-SSE trending basement ridge (Figure 3a, Mid-Shelf High; MSH), which comprises most of the shallowest (< 700 meters below sea level (mbsl) sub-RIS basement, with several regions having $< 50\text{m}$ sedimentary cover. Basement is deeper on the East Antarctic side of the MSH, where it averages ~ 2400 mbsl, compared to an average depth of ~ 1900 mbsl on the West Antarctic side (Figure 3a histogram). Sedimentary fill is $\sim 400\text{m}$ greater and more uniformly distributed on the East Antarctic side than the West Antarctic side (Figure 3b histogram).

To estimate our uncertainty, we examined the misfit between our basement and AN-TOSTRAT and OIB basement (Figures 2, S2, S3e&f, Text S6). There is a median misfit of 480m (22% of average depth) for basement. Incorporating the $\sim 70\text{m}$ uncertainty in the bathymetry model (Tinto et al., 2019), our sediment thickness uncertainty is 550m (37% of average thickness). A similar 480m basement misfit is estimated by comparing our results to eight active source seismic surveys (Figure 3b, Table S1).

A single broad and deep basin ($300 \times 600\text{km}$) separates the MSH and the Transantarctic Mountains (TAM) (Figure 3a, Western Ross Basin). The Western Ross Basin parallels the TAM and has the deepest-observed sub-RIS basement depths of 4500 mbsl, accommodating sediments up to 3800m thick (Figure 3b). It contains a long, narrow NW-SE trending ridge with $\sim 1500\text{m}$ structural relief above the basement sub-basins on either side. Bordering the MSH on the east, an elongate NW-SE trending basin runs from the RIS calving front to the Siple Coast GZ (Figure 3a), where beneath Siple Dome we discover a $100 \times 200\text{km}$ depocenter reaching basement depths up to 4000 mbsl, with sediments up to 3700m thick. We refer to this depocenter as Siple Dome Basin, a feature bounded on the east by a basement high that trends southward from Roosevelt Island. This high rises to its shallowest point at the GZ, where its sedimentary cover is less than 100m . A second deep, narrow basin ($50 \times 200\text{km}$ in dimension) is found along the north margin of Crary Ice Rise, separated from the Siple Dome Basin by a NW-SE ridge underlying Kamb Ice Stream. The basin, labeled Crary Trough in Figure 3a, reaches basement depths of 3200 mbsl, with sediments $1800\text{--}2700\text{m}$ thick. The southernmost RIS has an additional depocenter with up to 2000m of fill beneath Whillans Ice Stream (location in Figure 1a).

We inferred the locations of active and inactive sub-RIS faults (Figures 4a & S1). Active faults correspond to narrow, linear basement basins with high-gradient gravity anomalies, prevalent on the West Antarctic side (Figure S1a). Inactive normal and strike-slip faults are inferred along lineaments that segment the shallow MSH into blocks and are oriented parallel to TAM outlet glacier faults. β -factors are indicative of thinned crust and are different on either side of the MSH. The TAM side shows higher β -factors (average 1.99) with low variability. The West Antarctic side has lower β -factors overall (average 1.82), but with some higher values up to 2.1 (Figure 4a).

4 Discussion

Sub-RIS sedimentary basins align with and show lateral continuity with the Ross Sea's Roosevelt Sub-Basin, Eastern Basin, Coulman Trough, and Victoria Land Basin (Figure 3, e.g. Cooper et al., 1995). The MSH passes northward into the Ross Sea's prominent Central High (CH). At the southern RIS margin, the narrow Siple Dome Basin has continuity with the previously identified Trunk D Basin (Figure 3a, Bell et al., 2006). The throughgoing trends imply regional continuity of crustal structure and a common tectonic development of the Ross Sea and RIS regions. Our sediment thicknesses are compatible with those determined by a) eight active-source seismic surveys (Figure 3b), for

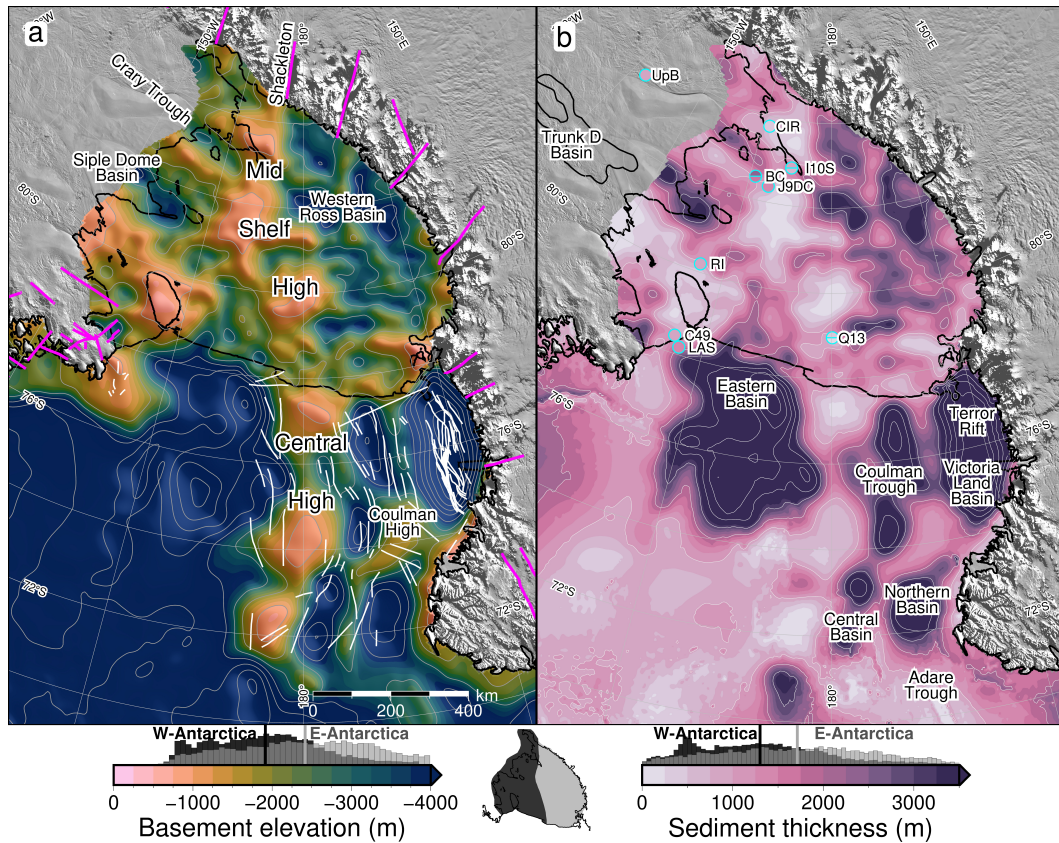


Figure 3. (a) Depth to basement (magnetic for Ross Ice Shelf (RIS), seismic elsewhere) contoured at 1km intervals. Pink lines are onshore mapped and inferred faults (Goode, 2020; Siddoway, 2008; Ferraccioli et al., 2002). White lines are offshore faults (Salvini et al., 1997; Luyendyk et al., 2001; Chiappini et al., 2002; Sauli et al., 2021). (b) Sediment thickness contoured at 1km intervals. Previous basement-imaging RIS seismic surveys (Table S1) are plotted on same color scale, with upper and lower uncertainty ranges as circle halves, where reported. Trunk D Basin outlined in West Antarctica (Bell et al., 2006). Color scales for both a) and b) are set to sub-RIS data range. Colorbar histograms show data distribution for East vs West Antarctic sides of the sub-RIS, separated by the Mid-Shelf High. Inset map shows East vs West divide. Vertical lines on histograms denote average values of each side.

166 which the median misfit is 480m (Table S1), and b) surface wave dispersion indicating
 167 2-4km of sediment under the RIS, similar to our range, with the maximum beneath Crary
 168 Ice Rise (Zhou et al., 2022). Three additional western RIS seismic profiles report up to
 169 several kilometers of sediment, in general accordance with our results (Stern et al., 1991;
 170 ten Brink et al., 1993; Beaudoin et al., 1992). Additionally, machine learning applied to
 171 geophysical datasets predicts a high likelihood of sedimentary basins at the locations of
 172 Siple Dome Basin and Crary Trough (L. Li et al., 2021).

173 **4.1 West Antarctic Rift System extensional basins**

174 The Western Ross Basin has a configuration similar to the western Ross Sea rift
 175 basins (e.g. Salvini et al., 1997) with a broad and deep basin, separated into distinct de-
 176 pocenters by a linear, low relief ridge. The deeper of the depocenters, on the TAM side
 177 of the ridge, coincides with a narrow gravity anomaly (Figure S1a). These similarities
 178 suggest the sub-RIS continuations of Coulman Trough and Victoria Land Basin (Fig-
 179 ure 3b) likely share a common tectonic origin as fault-controlled basins (Figures 3a &
 180 4a) formed through Cretaceous distributed continental extension across the WARS (Jordan
 181 et al., 2020). These sub-RIS basins terminate against the southern segment of the MSH
 182 (Figure 3a).

183 The linear ridge within the Western Ross Basin (Figure 3a) may be an expression
 184 of normal or oblique faults linked to the southward-narrowing Terror Rift (Sauli et al.,
 185 2021), formed due to Cenozoic oceanic spreading in the Adare Trough (Figure 3b, Gra-
 186 not & Dymant, 2018). The Western Ross Basin, with up to 3800m of fill, terminates along
 187 the prominent edge of the MSH that lines up with the fault-controlled trough and crustal
 188 boundary that passes southward beneath Shackleton Glacier (Borg et al., 1990). We in-
 189 terpret the basement lineament (Figure 4a) as a transfer fault separating sectors of crust
 190 extended to different degrees.

191 The southeastern RIS margin is distinguished by linear ridges and narrow, deep
 192 basins. The prominent NW-SE basement trends coincide with high-gradient gravity anoma-
 193 lies (Figure S1a, Tinto et al., 2019) and thick sediments, suggesting normal fault con-
 194 trol and active divergent tectonics beneath the GZ. Our Siple Coast cross-section (Fig-
 195 ure 4b) displays dramatic basement relief, exceeding 2km, in the Siple Dome Basin and
 196 Crary Trough, which we attribute to displacement upon high angle faults. Portions of
 197 basin-bounding faults were previously detected by ground-based gravity surveys upon
 198 the Whillans Ice Stream flank (Figure 4a, Muto et al., 2013) and site J9DC (Figure 3b),
 199 where large variations in sediment thickness indicate up to 600m of fault throw (Greischar
 200 et al., 1992). The continuity between the narrow Siple Dome Basin (this study) and the
 201 Trunk D Basin (Figure 3a, Bell et al., 2006) suggests that the active tectonic domain con-
 202 tinues southward past the GZ. The fault-controlled tectonic basins may be an expres-
 203 sion of a crustal response to the lithospheric foundering hypothesized beneath the South
 204 Pole region (Shen, Wiens, Stern, et al., 2018).

205 **4.2 Cryosphere-groundwater implications**

206 Fault juxtaposition of low-permeability basement next to permeable basin fill, in
 207 a subglacial setting, is likely to affect groundwater reservoir capacity and promote fluid
 208 overpressure of the ice sheet-confined aquifer (e.g. Ravier & Buoncristiani, 2018), with
 209 consequences for ice sheet processes (Christoffersen et al., 2014). The effects of deep vo-
 210 luminous groundwater within the sub-Whillans fault-controlled basin, discerned using
 211 magnetotellurics, are thought to influence ice streaming (Gustafson et al., 2021). Ground-
 212 water discharge and recharge along fault damage zones (Jolie et al., 2021) may influence
 213 the distribution of heat in the subglacial environment (Burton-Johnson et al., 2020). Mod-
 214 ulated by pressure from the overriding ice sheet (Gooch et al., 2016), upward movement
 215 and discharge of waters may deliver heat that induces basal melting. Alternatively, basin

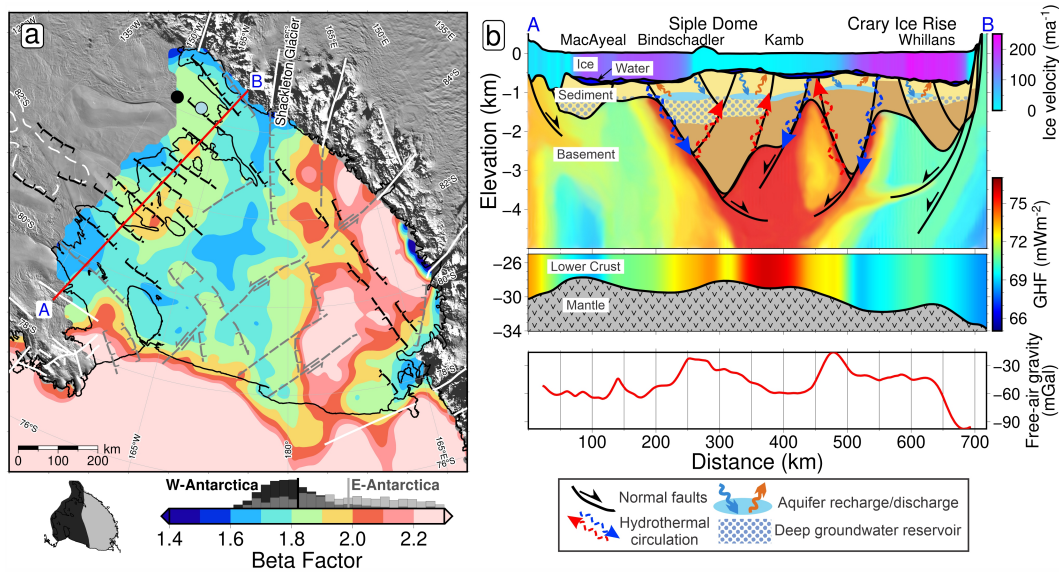


Figure 4. Tectonic interpretation of the sub-Ross Ice Shelf (RIS). **(a)** β stretching factors (Text S5), with sediments removed. Colorbar histogram shows data distribution of West vs. East Antarctic sides, same as Figure 3. Black and grey lines indicate inferred active and inactive faults, respectively, with kinematics shown with half-arrows (strike or oblique-slip) and hachures (normal-sense). White lines show previously reported faults, same as Figure 3a. Dashed-white outline is Trunk D Basin (Bell et al., 2006). Black and blue dots show Subglacial Lake Whillans and sedimentary basin from Gustafson et al. (2021), respectively. Cross-section A-B in red. **(b)** Siple Coast cross-section from A-B, showing basin sediments bounded by faults, with geothermal heat flux (GHF) through the crust (lower panel from Burton-Johnson et al. (2020), upper panel interpreted) with implications for subglacial hydrology. Ice surface, ice base, and bathymetry from Morlighem et al. (2020). Ice streams colored by velocity (Mouginot et al., 2019). Moho is from Shen, Wiens, Anandakrishnan, et al. (2018). Lower panel shows ROSETTA-Ice gravity. Named features are labeled on top.

216 recharge can sequester heat at lower depths within permeable basin fill. Regionally el-
 217 evated GHF modeled along the Siple Coast (Shen et al., 2020) and anomalously high GHF
 218 (285 mW/m^2) at Subglacial Lake Whillans (Figure 4a, Fisher et al., 2015) are likely the
 219 result of the active extensional setting and strong GHF localization upon faults bound-
 220 ing sedimentary basins. If this localization persists beneath the Siple Coast ice streams,
 221 it is likely to influence ice flow.

222 At a more regional scale, active graben-bounding faults likely accommodate rel-
 223 ative motion in response to changes in ice sheet volume along the Siple Coast, a region
 224 underlain by low-viscosity mantle (Whitehouse et al., 2019; Shen, Wiens, Anandakrish-
 225 nan, et al., 2018). In this region, Kingslake et al. (2018) found evidence of swift glacioiso-
 226 static rebound following Holocene deglaciation, with changes in bed elevation and ge-
 227 ometry producing a negative feedback (cf. Lowry et al., 2020; Coulon et al., 2021) that
 228 drove ice sheet re-advance and re-stabilized the ice sheet. The matter is receiving con-
 229 siderable debate (Neuhaus et al., 2021).

230 4.3 Central High - Mid-Shelf High

231 Using contrasts in crustal characteristics, including magnetic and gravity anom-
 232 alies, Tinto et al. (2019) identified a mid-Ross Embayment north-south trending geologic
 233 boundary separating crust of East and West Antarctic affinity. Geological substantia-
 234 tion comes from basement rock samples recovered from the CH at DSDP 270 (Ford &
 235 Barrett, 1975), and at Iselin Bank (Figure 3, Mortimer et al., 2011), which have litho-
 236 logic affinities to the TAM. The MSH in the magnetic basement coincides with this bound-
 237 ary, as does the Ross Sea’s CH, an association that is borne out by passive-seismic stud-
 238 ies that show the boundary to be present at lithospheric scale (Cheng et al., 2021; White-
 239 Gaynor et al., 2019). The distinct geologic properties on either side of the MSH related
 240 to West versus East Antarctic type crust (Tinto et al., 2019) appear to have controlled
 241 the respective responses to WARS extension. We determined high and homogeneous β -
 242 factors on the TAM-side, indicating distributed crustal extension. The West Antarctic
 243 side’s β -factors indicate lesser extension, but with specific sites of more extreme thin-
 244 ning (Figure 4a). The greater amount of extension on the East Antarctic side coincides
 245 with the deeper bathymetry (Figure 1a), deeper basement, and thicker sediments (Fig-
 246 ure 3).

247 The CH-MSH basement feature trends southward into the TAM, where its west-
 248 ern edge aligns with Shackleton Glacier, occupying a major fault separating the distinct
 249 geologic domains of the central and southern TAM (Borg et al., 1990; Paulsen et al., 2004).
 250 Previous authors noted the alignment of the Shackleton Glacier Fault, a 250-km long fault
 251 on the south side of the TAM (Drewry, 1972), and a prominent magnetic lineament at
 252 the South Pole (Studinger et al., 2006). This N-S sequence of structures may be an ex-
 253 pression of the East Antarctic craton margin or a major intracontinental transform (Figure
 254 4a, Studinger et al., 2006). The spatial correspondence of the East-West Antarctic ge-
 255 ologic boundary, the N-S series of linear features, and the prominent basement highs sug-
 256 gest the CH-MSH is a major tectonic feature that, through tectonic inheritance (Corti
 257 et al., 2007), has influenced the rift architecture and development of Ross Embayment.

258 Paleotopographic reconstructions of the early Oligocene depict a proto-Ross Em-
 259 bayment divided by a long, narrow mountain range (the MSH-CH), emergent above sea
 260 level (Paxman et al., 2019; Wilson et al., 2012), that hosted alpine glaciers and small ice
 261 caps (De Santis et al., 1995). These ice caps represent the initial glacial stage in the re-
 262 gion and once established, were the centers from which continental ice expanded to the
 263 outer Ross Sea continental shelf (Bart & De Santis, 2012). Between the late Oligocene
 264 and mid-Miocene, up to 500m of subsidence and sedimentation occurred (Leckie, 1983;
 265 Kulhanek et al., 2019) and the CH became covered in sediment (De Santis et al., 1995).
 266 The geophysical similarities and continuity between the Ross Sea’s CH and the RIS’s MSH

267 imply a similar glaciation and subsidence history for the RIS region as for the Ross Sea.
268 A terrestrial/alpine stage for the MSH helps to explain the region's potential to hold the
269 late Oligocene's larger-than-modern ice volumes (Wilson et al., 2013; Pekar et al., 2006).
270 Analysis of subglacial sediment identified a major ice flow divide between East and West
271 Antarctic ice since the Last Glacial Maximum (X. Li et al., 2020; Licht et al., 2014; Co-
272 enen et al., 2019). These findings highlight the CH-MSH as important features for both
273 Oligocene ice sheet development and the subsequent evolution of the ice sheet and ice
274 shelf, as documented in the Ross Sea (Halberstadt et al., 2016).

275 4.4 Thermal subsidence and sedimentation

276 Incorporating the updated basement basin extents and geometries into post-rift ther-
277 mal subsidence modeling will enable better constrained paleotopographic reconstructions.
278 For the sub-RIS, these reconstructions (Wilson et al., 2012; Paxman et al., 2019) use a
279 post-Eocene subsidence model based on gravity-derived basin geometries and uniform
280 β -factors (Wilson & Luyendyk, 2009). This model predicts uniform stretching of the east-
281 ern sub-RIS from the ice front to the Siple Coast, while our β -factors show increasing
282 stretching from the ice front to the Siple Coast. This observed additional thinning likely
283 has resulted in more subsidence for Siple Dome and the north flank of Crary Ice Rise,
284 which can now be accounted for in reconstructions. Our sediment thickness comparison
285 with past models (Text S5, Wilson & Luyendyk, 2009) shows the majority of the sub-
286 RIS, especially the Siple Coast, contains more total sediment than previously estimated
287 (Figure S1f). Depending on the age of this sediment, reconstructions may need to ac-
288 count for the additional sediment deposition and loading.

289 5 Conclusions

290 Here we present a depth to magnetic basement map for the Ross Ice Shelf (RIS)
291 from Werner deconvolution of airborne magnetics data. The RIS magnetic basement is
292 tied to Ross Sea seismic basement, providing the first synthetic view of Ross Embayment
293 crustal structure. Subtracting bathymetry, we obtain the sediment thickness distribu-
294 tion and calculate crustal extension factors for the sub-RIS. The extensional features we
295 image, resulting from West Antarctic Rift System extension, have continuity with Ross
296 Sea basement structures to the north, and the prominent Mid-Shelf High trends north-
297 ward into the Ross Sea's Central High. This combined high separates East and West Antarc-
298 tic type crust, affected by different degrees of continental extension. The Mid-Shelf High
299 was likely subaerial in the Oligocene, able to support alpine ice caps in early Antarctic
300 glaciation, and subsequently to form an ice flow divide between the East and West Antarc-
301 tic Ice Sheets. Newly identified narrow, linear, deep sedimentary basins provide evidence
302 of active faults beneath the Siple Coast grounding zone, where thinned crust overlying
303 anomalous mantle (Shen, Wiens, Anandakrishnan, et al., 2018) likely experiences ele-
304 vated geothermal heat flow promoting the formation of subglacial water. Faults that con-
305 trol basement margins may accommodate motion caused by the glacioisostatic response
306 to ice sheet volume changes. Subglacial sedimentary basins in this setting likely contain
307 confined aquifers with permeable basin fill. Here, ice overburden pressure would control
308 flow both between and within the subglacial and groundwater systems, possibly local-
309 izing geothermal heat. Updated sediment thickness and basin extent should be incor-
310 porated into new paleotopographic reconstructions of time intervals of interest for paleo-
311 ice sheet modeling. Our work contributes critical information about Ross Embayment
312 basement topography and subglacial boundary conditions that arise from an interplay
313 of geology, tectonics, and glaciation.

6 Open Research

ROSETTA-Ice and OIB magnetics data are available from <https://pgg.ldeo.columbia.edu/data>. Results from this study are available to download from <https://doi.pangaea.de/10.1594/PANGAEA.941238>. A Jupyter notebook documenting our workflow is available at <https://zenodo.org/badge/latestdoi/470814953>.

Acknowledgments

Funding support from the New Zealand Ministry of Business and Innovation and Employment through the Antarctic Science Platform contract (ANTA1801) Antarctic Ice Dynamics Project (ASP-021-01) and the National Science Foundation (1443497 and 1443534). We are grateful to Robin Bell, Isabel Cordero, Alec Lockett, Joel Wilner, Zoe Krauss, and the entire ROSETTA-Ice team for undertaking the ambitious data acquisition and processing effort. We thank Katharina Hochmuth and one anonymous reviewer for thoughtful reviews which greatly improved the manuscript, as well as Chris Sorlien, Tim Stern, Simon Lamb, Lara Pérez, Wei Ji Leong, and Dan Lowry for valuable input. Figures used GMT6/PyGMT (Wessel et al., 2019; Uieda et al., 2021), with a script adapted from Venturelli et al. (2020). Geosoft Oasis MontajTM was used for magnetics processing and Werner deconvolution.

References

- An, M., Wiens, D. A., Zhao, Y., Feng, M., Nyblade, A. A., Kanao, M., . . . Lévêque, J.-J. (2015). S-velocity model and inferred Moho topography beneath the Antarctic Plate from Rayleigh waves: Antarctic S-velocities and Moho. *Journal of Geophysical Research: Solid Earth*, *120*(1), 359–383. doi: 10.1002/2014JB011332
- Andrews, J. T., & LeMasurier, W. (2021). Resolving the argument about volcanic bedrock under the West Antarctic Ice Sheet and implications for ice sheet stability and sea level change. *Earth and Planetary Science Letters*, *568*, 117035. doi: 10.1016/j.epsl.2021.117035
- Austermann, J., Pollard, D., Mitrovica, J. X., Moucha, R., Forte, A. M., DeConto, R. M., . . . Raymo, M. E. (2015). The impact of dynamic topography change on Antarctic ice sheet stability during the mid-Pliocene warm period. *Geology*, *43*(10), 927–930. doi: 10.1130/G36988.1
- Bart, P., & De Santis, L. (2012). Glacial intensification during the Neogene: A review of seismic stratigraphic evidence from the Ross Sea, Antarctica, continental shelf. *Oceanography*, *25*(3), 166–183. doi: 10.5670/oceanog.2012.92
- Beaudoin, B. C., ten Brink, U. S., & Stern, T. A. (1992). Characteristics and processing of seismic data collected on thick, floating ice: Results from the Ross Ice Shelf, Antarctica. *Geophysics*, *57*(10), 1359–1372. doi: 10.1190/1.1443205
- Begeman, C. B., Tulaczyk, S. M., & Fisher, A. T. (2017). Spatially Variable Geothermal Heat Flux in West Antarctica: Evidence and Implications. *Geophysical Research Letters*, *44*(19), 9823–9832. doi: 10.1002/2017GL075579
- Bell, R. E., Ferraccioli, F., Creyts, T. T., Braaten, D., Corr, H., Das, I., . . . Wolovick, M. (2011). Widespread Persistent Thickening of the East Antarctic Ice Sheet by Freezing from the Base. *Science*, *331*(6024), 1592–1595. doi: 10.1126/science.1200109
- Bell, R. E., Studinger, M., Karner, G., Finn, C. A., & Blankenship, D. D. (2006). Identifying major sedimentary basins beneath the West Antarctic Ice Sheet from aeromagnetic data analysis. In D. K. Fütterer, D. Damaske, G. Kleinschmidt, H. Miller, & F. Tessensohn (Eds.), *Antarctica* (pp. 117–121). Berlin/Heidelberg: Springer-Verlag. doi: 10.1007/3-540-32934-X_13
- Birch, F. (1984). Bedrock depth estimates from ground magnetometer profiles Werner deconvolution. *Ground Water*, *22*(4), 427–432. doi: 10.1111/j.1745-6584.1984.tb01413.x

- 365 Borg, S. G., Depaolo, D. J., & Smith, B. M. (1990). Isotopic structure and tectonics of the central Transantarctic mountains. *Journal of Geophysical Research*, 95(B5), 6647. doi: 10.1029/JB095iB05p06647
- 366
367
- 368 Brancolini, G., Busetti, M., Marchetti, A., Santis, L. D., Zanolla, C., Cooper, A. K.,
369 ... Hinze, K. (1995). Descriptive text for the seismic stratigraphic atlas of
370 the Ross Sea, Antarctica. In A. K. Cooper, P. F. Barker, & G. Brancolini
371 (Eds.), *Geology and Seismic Stratigraphy of the Antarctic Margin* (Vol. 68,
372 p. A271-A286). Washington, D. C.: American Geophysical Union. doi:
373 10.1002/9781118669013.app1
- 374 Burton-Johnson, A., Dziadek, R., & Martin, C. (2020). Geothermal heat flow in
375 Antarctica: Current and future directions. *The Cryosphere Discussions*, 1–45.
376 doi: 10.5194/tc-2020-59
- 377 Cheng, W., Hu, X. G., & Liu, L. T. (2021). Anisotropy Gradients in the Middle of
378 the Ross Sea Embayment, West Antarctica: Evidence From QL Scattered Sur-
379 face Waves. *Geophysical Research Letters*, 48(6). doi: 10.1029/2020GL091232
- 380 Chiappini, M., Ferraccioli, F., Bozzo, E., & Damaske, D. (2002). Regional compi-
381 lation and analysis of aeromagnetic anomalies for the Transantarctic Moun-
382 tains–Ross Sea sector of the Antarctic. *Tectonophysics*, 347(1-3), 121–137. doi:
383 10.1016/S0040-1951(01)00241-4
- 384 Christoffersen, P., Bougamont, M., Carter, S. P., Fricker, H. A., & Tulaczyk, S.
385 (2014). Significant groundwater contribution to Antarctic ice streams hy-
386 drologic budget. *Geophysical Research Letters*, 41(6), 2003–2010. doi:
387 10.1002/2014GL059250
- 388 Cochran, J. R., Burton, B., Frearson, N., & Tinto, K. (2014). IceBridge Scintrex
389 CS-3 Cesium magnetometer LIB geolocated magnetic anomalies, version 2.
390 [Line 403, 404]. Boulder, Colorado USA. NASA National Snow and Ice Data
391 Center Distributed Active Archive Center. doi: 10.5067/OY7C2Y61YSYW
- 392 Coenen, J. J., Scherer, R. P., Baudoin, P., Warny, S., Castañeda, I. S., & Askin,
393 R. (2019). Paleogene marine and terrestrial development of the West
394 Antarctic Rift System. *Geophysical Research Letters*, 47(3). doi: 10.1029/
395 2019GL085281
- 396 Colleoni, F., De Santis, L., Montoli, E., Olivo, E., Sorlien, C. C., Bart, P. J., ...
397 Prato, S. (2018). Past continental shelf evolution increased Antarctic ice
398 sheet sensitivity to climatic conditions. *Scientific Reports*, 8(1), 11323. doi:
399 10.1038/s41598-018-29718-7
- 400 Cooper, A. K., Barker, P. F., & Brancolini, G. (Eds.). (1995). *Geology and seismic*
401 *stratigraphy of the Antarctic margin* (No. v. 68). Washington, D.C: AGU. doi:
402 10.1029/AR068
- 403 Corti, G., van Wijk, J., Cloetingh, S., & Morley, C. K. (2007). Tectonic inheritance
404 and continental rift architecture: Numerical and analogue models of the East
405 African Rift system. *Tectonics*, 26(6), 1–13. doi: 10.1029/2006TC002086
- 406 Coulon, V., Bulthuis, K., Whitehouse, P. L., Sun, S., Haubner, K., Zipf, L., & Pat-
407 tyn, F. (2021). Contrasting response of West and East Antarctic Ice Sheets to
408 glacial isostatic adjustment. *Journal of Geophysical Research: Earth Surface*,
409 126(7). doi: 10.1029/2020JF006003
- 410 Cox, S., Smith Lyttle, B., & 2019, S. G. A. G. (2019). SCAR GeoMAP dataset.
411 *GNS Science*. doi: 10.21420/7SH7-6K05
- 412 Crary, A. P. (1961). Marine-sediment thickness in the eastern Ross Sea area, Antarc-
413 tica. *Geological Society of America Bulletin*, 72(5), 787. doi: 10.1130/0016-
414 -7606(1961)72[787:MTITER]2.0.CO;2
- 415 DeConto, R. M., & Pollard, D. (2003). A coupled climate–ice sheet mod-
416 eling approach to the Early Cenozoic history of the Antarctic ice sheet.
417 *Palaeogeography, Palaeoclimatology, Palaeoecology*, 198(1-2), 39–52. doi:
418 10.1016/S0031-0182(03)00393-6
- 419 De Santis, L., Anderson, J. B., Brancolini, G., & Zayatz, I. (1995). Seismic record

- 420 of late Oligocene through Miocene glaciation on the central and eastern conti-
 421 nental shelf of the Ross Sea. In A. K. Cooper, P. F. Barker, & G. Brancolini
 422 (Eds.), *Antarctic Research Series* (pp. 235–260). Washington, D. C.: American
 423 Geophysical Union. doi: 10.1029/AR068p0235
- 424 Drenth, B. J., Grauch, V., Turner, K. J., Rodriguez, B. D., Thompson, R. A., &
 425 Bauer, P. W. (2019). A shallow rift basin segmented in space and time: The
 426 southern San Luis Basin, Rio Grande rift, northern New Mexico, U.S.A. *Rocky*
 427 *Mountain Geology*, *54*(2), 97–131. doi: 10.24872/rmgjournal.54.2.97
- 428 Drewry, D. (1972). Subglacial morphology between the Transantarctic Mountains
 429 and the South Pole. In R. Adie (Ed.), *Antarctic Geology and Geophysics*
 430 (Vol. 1, pp. 693–703). Oslo: International Union of Geological Science. doi:
 431 10.26153/tsw/2786
- 432 Ferraccioli, F., Bozzo, E., & Damaske, D. (2002). Aeromagnetic signatures over
 433 western Marie Byrd Land provide insight into magmatic arc basement, mafic
 434 magmatism and structure of the Eastern Ross Sea Rift flank. *Tectonophysics*,
 435 *347*, 139–165. doi: 10.1016/S0040-1951(01)00242-6
- 436 Finn, C. (2002). *Examples of the utility of magnetic anomaly data for geologic map-*
 437 *ping* (Open-File Report No. 02-400). Denver, Colorado: USGS.
- 438 Fisher, A. T., Mankoff, K. D., Tulaczyk, S. M., Tyler, S. W., Foley, N., & and
 439 the WISSARD Science Team. (2015). High geothermal heat flux mea-
 440 sured below the West Antarctic Ice Sheet. *Science Advances*, *1*, 1–9. doi:
 441 10.1126/sciadv.1500093
- 442 Ford, A., & Barrett, P. J. (1975). *Basement rocks of the south-central Ross Sea, site*
 443 *270, DSDP leg 28* (Tech. Rep.). College Station, TX, United States: Texas A
 444 & M University, Ocean Drilling Program. doi: 10.2973/dsdp.proc.28.130.1975
- 445 Frederick, B. C., Young, D. A., Blankenship, D. D., Richter, T. G., Kempf, S. D.,
 446 Ferraccioli, F., & Siegert, M. J. (2016). Distribution of subglacial sediments
 447 across the Wilkes Subglacial Basin, East Antarctica. *Journal of Geophysical*
 448 *Research: Earth Surface*, *121*(4), 790–813. doi: 10.1002/2015JF003760
- 449 Fretwell, P., Pritchard, H. D., Vaughan, D. G., Bamber, J. L., Barrand, N. E.,
 450 Bell, R. E., ... Zirizzotti, A. (2013). Bedmap2: Improved ice bed, surface
 451 and thickness datasets for Antarctica. *The Cryosphere*, *7*(1), 375–393. doi:
 452 10.5194/tc-7-375-2013
- 453 Gooch, B. T., Young, D. A., & Blankenship, D. D. (2016). Potential groundwater
 454 and heterogeneous heat source contributions to ice sheet dynamics in critical
 455 submarine basins of East Antarctica. *Geochemistry, Geophysics, Geosystems*,
 456 *17*(2), 395–409. doi: 10.1002/2015GC006117
- 457 Goodge, J. W. (2020). Geological and tectonic evolution of the Transantarctic
 458 Mountains, from ancient craton to recent enigma. *Gondwana Research*, *80*,
 459 50–122. doi: 10.1016/j.gr.2019.11.001
- 460 Granot, R., & Dymant, J. (2018). Late Cenozoic unification of East and
 461 West Antarctica. *Nature Communications*, *9*(1), 3189. doi: 10.1038/
 462 s41467-018-05270-w
- 463 Greischar, L. L., Bentley, C. R., & Whiting, L. R. (1992). An analysis of gravity
 464 measurements on the Ross Ice Shelf, Antarctica. In *Contributions to Antarc-*
 465 *tic Research III* (pp. 105–155). American Geophysical Union (AGU). doi: 10
 466 .1029/AR057p0105
- 467 Gustafson, C., Key, K., Siegfried, M., Winberry, J. P., Fricker, H. A., Venturelli, R.,
 468 & Michaud, A. B. (2021). A deep and dynamic groundwater system beneath
 469 an Antarctic ice stream. In *AGU Fall Meeting 2021*. AGU.
- 470 Halberstadt, A. R. W., Simkins, L. M., Greenwood, S. L., & Anderson, J. B.
 471 (2016). Past ice-sheet behaviour: Retreat scenarios and changing con-
 472 trols in the Ross Sea, Antarctica. *The Cryosphere*, *10*(3), 1003–1020. doi:
 473 10.5194/tc-10-1003-2016
- 474 Jolie, E., Scott, S., Faulds, J., Chambefort, I., Axelsson, G., Gutiérrez-Negrín, L. C.,

- 475 ... Zemedkun, M. T. (2021). Geological controls on geothermal resources for
 476 power generation. *Nature Reviews Earth & Environment*, *2*(5), 324–339. doi:
 477 10.1038/s43017-021-00154-y
- 478 Jordan, T. A., Riley, T. R., & Siddoway, C. S. (2020). The geological history and
 479 evolution of West Antarctica. *Nature Reviews Earth & Environment*, *1*, 117–
 480 133. doi: 10.1038/s43017-019-0013-6
- 481 Karner, G. D., Studinger, M., & Bell, R. E. (2005). Gravity anomalies of sedimen-
 482 tary basins and their mechanical implications: Application to the Ross Sea
 483 basins, West Antarctica. *Earth and Planetary Science Letters*, *235*, 577–596.
 484 doi: 10.1016/j.epsl.2005.04.016
- 485 Kingslake, J., Scherer, R. P., Albrecht, T., Coenen, J., Powell, R. D., Reese, R.,
 486 ... Whitehouse, P. L. (2018). Extensive retreat and re-advance of the West
 487 Antarctic Ice Sheet during the Holocene. *Nature*, *558*(7710), 430–434. doi:
 488 10.1038/s41586-018-0208-x
- 489 Ku, C. C., & Sharp, J. A. (1983). Werner deconvolution for automated magnetic
 490 interpretation and its refinement using Marquardt’s inversion modeling. *Geo-*
 491 *physics*, *48*(6), 754–774.
- 492 Kulhanek, D. K., Levy, R. H., Clowes, C. D., Prebble, J. G., Rodelli, D., Jo-
 493 vane, L., ... Naish, T. R. (2019). Revised chronostratigraphy of DSDP
 494 Site 270 and late Oligocene to early Miocene paleoecology of the Ross Sea
 495 sector of Antarctica. *Global and Planetary Change*, *178*, 46–64. doi:
 496 10.1016/j.gloplacha.2019.04.002
- 497 Leckie, F. M. (1983). Late Oligocene-early Miocene glacial record of the Ross Sea,
 498 Antarctica: Evidence from DSDP Site 270. *Geology*, *11*, 578–582. doi: 10
 499 .1130/0091-7613(1983)11(578:LOMGRO)2.0.CO;2
- 500 Li, L., Aitken, A., Lindsay, M., & Kulesa, B. (2021). *Subglacial sedimentary basins*
 501 *focus key vulnerabilities of the Antarctic ice-sheet* (Preprint). In Review. doi:
 502 10.21203/rs.3.rs-1117673/v1
- 503 Li, X., Zattin, M., & Olivetti, V. (2020). Apatite fission track signatures of the Ross
 504 Sea ice flows during the Last Glacial Maximum. *Geochemistry, Geophysics,*
 505 *Geosystems*, *21*(10), 1–21. doi: 10.1029/2019GC008749
- 506 Licht, K. J., Hennessy, A. J., & Welke, B. M. (2014). The U-Pb detrital zircon
 507 signature of West Antarctic ice stream tills in the Ross embayment, with
 508 implications for Last Glacial Maximum ice flow reconstructions. *Antarctic*
 509 *Science*, *26*(6), 687–697. doi: 10.1017/S0954102014000315
- 510 Lindeque, A., Gohl, K., Wobbe, F., & Uenzelmann-Neben, G. (2016). Preglacial
 511 to glacial sediment thickness grids for the Southern Pacific Margin of West
 512 Antarctica: Preglacial, transitional and full glacial isopach maps, West Antarc-
 513 tica. *Geochemistry, Geophysics, Geosystems*, *17*(10), 4276–4285. doi:
 514 10.1002/2016GC006401
- 515 Lowry, D. P., Golledge, N. R., Bertler, N. A., Jones, R. S., McKay, R., & Stutz, J.
 516 (2020). Geologic controls on ice sheet sensitivity to deglacial climate forcing in
 517 the Ross Embayment, Antarctica. *Quaternary Science Advances*, *1*, 1–17. doi:
 518 10.1016/j.qsa.2020.100002
- 519 Luyendyk, B., Sorlien, C. C., Wilson, D. S., Bartek, L. R., & Siddoway, C. S.
 520 (2001). Structural and tectonic evolution of the Ross Sea rift in the Cape
 521 Colbeck region, Eastern Ross Sea, Antarctica. *Tectonics*, *20*(6), 933–958. doi:
 522 10.1029/2000TC001260
- 523 Luyendyk, B., Wilson, D. S., & Siddoway, C. S. (2003). Eastern margin of the Ross
 524 Sea Rift in western Marie Byrd Land, Antarctica: Crustal structure and tec-
 525 tonic development. *Geochemistry, Geophysics, Geosystems*, *4*(10), 1–25. doi:
 526 10.1029/2002GC000462
- 527 Mooney, W. D., Laske, G., & Masters, T. G. (1998). CRUST 5.1: A global crustal
 528 model at 5° × 5°. *Journal of Geophysical Research: Solid Earth*, *103*(B1), 727–
 529 747. doi: 10.1029/97JB02122

- 530 Morlighem, M., Rignot, E., Binder, T., Blankenship, D., Drews, R., Eagles, G., ...
 531 Young, D. A. (2020). Deep glacial troughs and stabilizing ridges unveiled
 532 beneath the margins of the Antarctic ice sheet. *Nature Geoscience*, *13*(2),
 533 132–137. doi: 10.1038/s41561-019-0510-8
- 534 Mortimer, N., Palin, J., Dunlap, W., & Hauff, F. (2011). Extent of the Ross Orogen
 535 in Antarctica: New data from DSDP 270 and Iselin Bank. *Antarctic Science*,
 536 *23*(3), 297–306. doi: 10.1017/S0954102010000969
- 537 Mouginot, J., Rignot, E., & Scheuchl, B. (2019). Continent-wide, interferometric
 538 SAR phase, mapping of Antarctic ice velocity. *Geophysical Research Letters*,
 539 *46*(16), 9710–9718. doi: 10.1029/2019GL083826
- 540 Müller, R. D., Gohl, K., Cande, S. C., Goncharov, A., & Golynsky, A. V. (2007).
 541 Eocene to Miocene geometry of the West Antarctic Rift System. *Aus-
 542 tralian Journal of Earth Sciences*, *54*(8), 1033–1045. doi: 10.1080/
 543 08120090701615691
- 544 Muto, A., Christianson, K., Horgan, H. J., Anandakrishnan, S., & Alley, R. B.
 545 (2013). Bathymetry and geological structures beneath the Ross Ice Shelf at the
 546 mouth of Whillans Ice Stream, West Antarctica, modeled from ground-based
 547 gravity measurements. *Journal of Geophysical Research: Solid Earth*, *118*(8),
 548 4535–4546. doi: 10.1002/jgrb.50315
- 549 Neuhaus, S. U., Tulaczyk, S. M., Stansell, N. D., Coenen, J. J., Scherer, R. P.,
 550 Mikucki, J. A., & Powell, R. D. (2021). Did Holocene climate changes
 551 drive West Antarctic grounding line retreat and readvance? *The Cryosphere*,
 552 *15*(10), 4655–4673. doi: 10.5194/tc-15-4655-2021
- 553 Paulsen, T., Encarnación, J., & Grunow, A. (2004). Structure and timing of
 554 transpressional deformation in the Shackleton Glacier area, Ross orogen,
 555 Antarctica. *Journal of the Geological Society*, *161*(6), 1027–1038. doi:
 556 10.1144/0016-764903-040
- 557 Paxman, G. J. G., Jamieson, S. S., Hochmuth, K., Gohl, K., Bentley, M. J.,
 558 Leitchenkov, G., & Ferraccioli, F. (2019). Reconstructions of Antarctic to-
 559 pography since the Eocene–Oligocene boundary. *Palaeogeography, Palaeoclima-
 560 tology, Palaeoecology*, *535*, 109346. doi: 10.1016/j.palaeo.2019.109346
- 561 Pekar, S. F., DeConto, R. M., & Harwood, D. M. (2006). Resolving a late
 562 Oligocene conundrum: Deep-sea warming and Antarctic glaciation. *Palaeo-
 563 geography, Palaeoclimatology, Palaeoecology*, *231*, 29–40. doi: 10.1016/
 564 j.palaeo.2005.07.024
- 565 Pérez, L. F., De Santis, L., McKay, R. M., Larter, R. D., Ash, J., Bart, P. J., ...
 566 374 Scientists, I. O. D. P. E. (2021). Early and middle Miocene ice sheet
 567 dynamics in the Ross Sea: Results from integrated core-log-seismic interpreta-
 568 tion. *GSA Bulletin*. doi: 10.1130/B35814.1
- 569 Ravier, E., & Buoncristiani, J.-F. (2018). Glaciohydrogeology. In *Past Glacial Envi-
 570 ronments* (pp. 431–466). Elsevier. doi: 10.1016/B978-0-08-100524-8.00013-0
- 571 Rignot, E., Jacobs, S., Mouginot, J., & Scheuchl, B. (2013). Ice-Shelf Melt-
 572 ing Around Antarctica. *Science*, *341*(6143), 266–270. doi: 10.1126/
 573 science.1235798
- 574 Robertson, J. D., & Bentley, C. R. (1989). The Ross Ice Shelf: Glaciology and geo-
 575 physics paper 3: Seismic studies on the grid western half of the Ross Ice Shelf:
 576 RIGGS I and RIGGS II. In C. R. Bentley & D. E. Hayes (Eds.), *Antarctic Re-
 577 search Series* (Vol. 42, pp. 55–86). Washington, D. C.: American Geophysical
 578 Union. doi: 10.1029/AR042p0055
- 579 Rooney, S. T., Blankenship, D. D., & Bentley, C. R. (1987). Seismic refraction
 580 measurements of crustal structure in West Antarctica. In G. D. McKenzie
 581 (Ed.), *Geophysical Monograph Series* (pp. 1–7). Washington, D. C.: American
 582 Geophysical Union. doi: 10.1029/GM040p0001
- 583 Salvini, F., Brancolini, G., Buseti, M., Storti, F., Mazzarini, F., & Coren, F. (1997).
 584 Cenozoic geodynamics of the Ross Sea region, Antarctica: Crustal extension,

- 585 intraplate strike-slip faulting, and tectonic inheritance. *Journal of Geophysical*
 586 *Research: Solid Earth*, 102(B11), 24669–24696. doi: 10.1029/97JB01643
- 587 Sauli, C., Sorlien, C., Buseti, M., De Santis, L., Geletti, R., Wardell, N., &
 588 Luyendyk, B. P. (2021). Neogene development of the Terror Rift, western
 589 Ross Sea, Antarctica. *Geochemistry, Geophysics, Geosystems*, 22(3). doi:
 590 10.1029/2020GC009076
- 591 Scambos, T., Haran, T., Fahnestock, M., Painter, T., & Bohlander, J. (2007).
 592 MODIS-based Mosaic of Antarctica (MOA) data sets: Continent-wide surface
 593 morphology and snow grain size. *Remote Sensing of Environment*, 111(2-3),
 594 242–257. doi: 10.1016/j.rse.2006.12.020
- 595 Shen, W., Wiens, D. A., Anandkrishnan, S., Aster, R. C., Gerstoft, P., Bromirski,
 596 P. D., ... Winberry, J. P. (2018). The crust and upper mantle structure of
 597 Central and West Antarctica from bayesian inversion of Rayleigh wave and
 598 receiver functions. *Journal of Geophysical Research: Solid Earth*, 123(9),
 599 7824–7849. doi: 10.1029/2017JB015346
- 600 Shen, W., Wiens, D. A., Lloyd, A. J., & Nyblade, A. A. (2020). A geothermal heat
 601 flux map of Antarctica empirically constrained by seismic structure. *Geophysi-*
 602 *cal Research Letters*, 47(14). doi: 10.1029/2020GL086955
- 603 Shen, W., Wiens, D. A., Stern, T., Anandkrishnan, S., Aster, R. C., Dalziel, I., ...
 604 Winberry, J. P. (2018). Seismic evidence for lithospheric foundering beneath
 605 the southern Transantarctic Mountains, Antarctica. *Geology*, 46(1), 71–74.
 606 doi: 10.1130/G39555.1
- 607 Siddoway, C. S. (2008). Tectonics of the West Antarctic Rift System: New
 608 light on the history and dynamics of distributed intracontinental exten-
 609 sion. In A. K. Cooper et al. (Eds.), *Antarctica: A Keystone in a Chang-*
 610 *ing World*. Washington DC: The National Academies Press. doi: 10.3133/
 611 ofr20071047KP09
- 612 Siegert, M. J., Kulesa, B., Bougamont, M., Christoffersen, P., Key, K., Andersen,
 613 K. R., ... Smith, A. M. (2018). Antarctic subglacial groundwater: A con-
 614 cept paper on its measurement and potential influence on ice flow. *Geological*
 615 *Society, London, Special Publications*, 461(1), 197–213. doi: 10.1144/SP461.8
- 616 Smith, W. H. F., & Wessel, P. (1990). Gridding with continuous curvature splines in
 617 tension. *GEOPHYSICS*, 55(3), 293–305. doi: 10.1190/1.1442837
- 618 Sorlien, C. C., Luyendyk, B., Wilson, D. S., Decesari, R. C., Bartek, L. R., &
 619 Diebold, J. B. (2007). Oligocene development of the West Antarctic
 620 Ice Sheet recorded in eastern Ross Sea strata. *Geology*, 35(5), 467. doi:
 621 10.1130/G23387A.1
- 622 Stern, T. A., Davey, F. J., & Delisle, G. (1991). Lithospheric flexure induced by the
 623 load of the Ross Archipelago, southern Victoria land, Antarctica. In M. Thom-
 624 son, A. Crame, & J. Thomson (Eds.), *Geological Evolution of Antarctica* (pp.
 625 323–328). Cambridge, UK: Cambridge University Press.
- 626 Still, H., Campbell, A., & Hulbe, C. (2019). Mechanical analysis of pinning points
 627 in the Ross Ice Shelf, Antarctica. *Annals of Glaciology*, 60(78), 32–41. doi: 10
 628 .1017/aog.2018.31
- 629 Studinger, M., Bell, R., Fitzgerald, P., & Buck, W. (2006). Crustal architecture of
 630 the Transantarctic Mountains between the Scott and Reedy Glacier region and
 631 South Pole from aerogeophysical data. *Earth and Planetary Science Letters*,
 632 250(1-2), 182–199. doi: 10.1016/j.epsl.2006.07.035
- 633 Studinger, M., Bell, R. E., Buck, W., Karner, G. D., & Blankenship, D. D. (2004).
 634 Sub-ice geology inland of the Transantarctic Mountains in light of new aero-
 635 geophysical data. *Earth and Planetary Science Letters*, 220(3-4), 391–408. doi:
 636 10.1016/S0012-821X(04)00066-4
- 637 ten Brink, U. S., Bannister, S., Beaudoin, B. C., & Stern, T. A. (1993). Geophysical
 638 investigations of the tectonic boundary between East and West Antarctica.
 639 *Science*, 261(5117), 45–50. doi: 10.1126/science.261.5117.45

- 640 Tinto, K. J., Padman, L., Siddoway, C. S., Springer, S. R., Fricker, H. A., Das, I.,
641 ... Bell, R. E. (2019). Ross Ice Shelf response to climate driven by the tec-
642 tonic imprint on seafloor bathymetry. *Nature Geoscience*, *12*(6), 441–449. doi:
643 10.1038/s41561-019-0370-2
- 644 Uieda, L., Tian, D., Leong, W. J., Jones, M., Schlitzer, W., Toney, L., ... Quinn, J.
645 (2021). *PyGMT: A Python interface for the Generic Mapping Tools*. Zenodo.
646 doi: 10.5281/zenodo.5607255
- 647 Venturelli, R. A., Siegfried, M. R., Roush, K. A., Li, W., Burnett, J., Zook, R., ...
648 Rosenheim, B. E. (2020). Mid-Holocene grounding line retreat and read-
649 vance at Whillans Ice Stream, West Antarctica. *Geophysical Research Letters*,
650 *47*(15). doi: 10.1029/2020GL088476
- 651 Werner, S. (1953). Interpretation of magnetic anomalies at sheet-like bodies. In
652 *Sveriges Geologiska Undersok* (pp. 413–449). Stockholm Norstedt.
- 653 Wessel, P., Luis, J. F., Uieda, L., Scharroo, R., Wobbe, F., Smith, W. H. F., & Tian,
654 D. (2019). The Generic Mapping Tools version 6. *Geochemistry, Geophysics,*
655 *Geosystems*, *20*(11), 5556–5564. doi: 10.1029/2019GC008515
- 656 White-Gaynor, A. L., Nyblade, A. A., Aster, R. C., Wiens, D. A., Bromirski, P. D.,
657 Gerstoft, P., ... Anandakrishnan, S. (2019). Heterogeneous upper man-
658 tle structure beneath the Ross Sea Embayment and Marie Byrd Land, West
659 Antarctica, revealed by P-wave tomography. *Earth and Planetary Science*
660 *Letters*, *513*, 40–50. doi: 10.1016/j.epsl.2019.02.013
- 661 Whitehouse, P. L., Gomez, N., King, M. A., & Wiens, D. A. (2019). Solid Earth
662 change and the evolution of the Antarctic Ice Sheet. *Nature Communications*,
663 *10*(1), 503. doi: 10.1038/s41467-018-08068-y
- 664 Wilson, D. S., Jamieson, S. S., Barrett, P. J., Leitchenkov, G., Gohl, K., & Larter,
665 R. D. (2012). Antarctic topography at the Eocene–Oligocene boundary.
666 *Palaeogeography, Palaeoclimatology, Palaeoecology*, *335–336*, 24–34. doi:
667 10.1016/j.palaeo.2011.05.028
- 668 Wilson, D. S., & Luyendyk, B. (2009). West Antarctic paleotopography estimated at
669 the Eocene–Oligocene climate transition. *Geophysical Research Letters*, *36*(16),
670 L16302. doi: 10.1029/2009GL039297
- 671 Wilson, D. S., Pollard, D., DeConto, R. M., Jamieson, S. S., & Luyendyk, B. (2013).
672 Initiation of the West Antarctic Ice Sheet and estimates of total Antarctic
673 ice volume in the earliest Oligocene. *Geophysical Research Letters*, *40*(16),
674 4305–4309. doi: 10.1002/grl.50797
- 675 Zhou, Z., Wiens, D. A., Shen, W., Aster, R. C., Nyblade, A., & Wilson, T. J.
676 (2022). Radial Anisotropy and Sediment Thickness of West and Central
677 Antarctica Estimated From Rayleigh and Love Wave Velocities. *Journal of*
678 *Geophysical Research: Solid Earth*, *127*(3). doi: 10.1029/2021JB022857